Enhanced photocatalytic degradation of levofloxacin over heterostructured C$_3$N$_4$/Nb$_2$O$_5$ system under visible light

Muhammad Imran Rameel [a,1], Mehar Wali [a,1], Jehan Y. Al-Humaidi [b,**], Faroha Liaqat [c], Muhammad Abdullah Khan [a,*]

[a] *Renewable Energy Advancement Laboratory (REAL), Department of Environmental Sciences, Quaid-i-Azam University Islamabad, Pakistan*
[b] *Department of Chemistry College of Science Princess Nourah bint Abdulrahman University. P.O. BOX 84428, Riyadh 11671, Saudi Arabia*
[c] *Department of Chemistry, Quaid-i-Azam University Islamabad, Pakistan*

ARTICLE INFO

ABSTRACT

The growing usage of antibiotics and their subsequent release in water bodies have become a serious environmental concern. In this study, heterostructured photocatalysts C$_3$N$_4$/Nb$_2$O$_5$ have been synthesized using a simple hydrothermal method and applied to facilitate the degradation of the widely used antibiotic levofloxacin. The structural, morphological, and optical properties of the photocatalysts were characterized using XRD, SEM, TEM, UV–Vis and PL to establish the structure-property relationship. The type-II heterojunctions C$_3$N$_4$/Nb$_2$O$_5$ show remarkable activity under visible light irradiation, where Nb$_2$O$_5$ facilitates preferential adsorption of levofloxacin at the catalyst surface while C$_3$N$_4$ extends visible light absorption. This synergy resulted in superior catalytic performance (91%) in the optimized system, exceeding that of individual materials (Nb$_2$O$_5$ 30% and C$_3$N$_4$ 56%). The effect of catalyst dosage, pH, oxygen and point of zero is also investigated. The process is mainly photo-driven, and the trapping experiments reveal superoxide radicals as key species responsible for the degradation. Additionally, the adsorption behaviour, reformation of the degraded pollutant and reusability factors are evaluated to assess the practical feasibility of the photocatalytic system.

1. Introduction

Antibiotics are widely used chemicals that are resistant to breakdown in natural conditions [1]. One pervasive category of antibiotics, fluoroquinolones (FQ), reported in aquatic ecosystems, are constantly highlighted as emerging environmental contaminants [2–4]. It has been reported that approximately 70% of the administered antibiotics are excreted in their active form into the environment, contributing to their accumulation in the ecosystem [3,5]. The primary sources of FQs buildup in the environment are wastewater discharge from healthcare facilities, pharmaceutical manufacturing, and agricultural runoff. Notably, the overuse of levofloxacin as an anti-inflammatory drug for humans has increased residual groundwater concentrations [6,7]. Levofloxacin exhibits a broad spectrum of activity and has a prolonged half-life, making it difficult to degrade its active pharmaceutical ingredients, rendering conventional treatment methods ineffective, ultimately compromising drinking water safety [8,9]. Consequently, advanced

---

oxidation processes (AOPs), such as ozonation, photo-Fenton reaction, electrochemical treatment, and photocatalysis, are actively sought to mitigate the risk of levofloxacin contamination in the environment [10–13].

Among the AOPs, photocatalysis has attracted much attention due to its sustainable nature and environment friendly operation [14–17]. It employs metal oxide semiconductors and light to generate active species such as electron holes and radicals at the surface of the photocatalyst to drive chemical reactions. Traditional metal oxide semiconductors such as TiO_2, ZnO, and Nb_2O_5 etc., are only active in UV light, which constitutes 4% of solar light and thus limits higher quantum yields [18,19]. Such single semiconductors systems lack supplementary energy levels for charge species and usually display high recombination rates. To address this issue, several approaches have been explored to deter energy-wasteful recombination by constructing heterojunctions that provide additional energy levels for charge carriers [20]. These approaches include the formation of phase heterojunctions by combining two different crystal phases of a single semiconductor and heterojunctions constructed by coupling two different semiconductors to improve the catalytic activity [21–24]. However, phase heterojunctions owing to intrinsic structural rigidity have the limitation of extending absorption regimes [25,26]. In comparison, coupling two well-matched semiconductors to construct heterojunctions can be a promising approach for achieving desired band structure and -absorption range for photocatalysis applications.

To broaden the absorption spectrum of Nb_2O_5, strategies have been developed to modify the electronic structure through metal doping, such as Rh and Pb. Heterostructured systems involving Nb_2O_5, such as Nb_2O_5/CuO, Nb_2O_5/ZnO, TiO_2/Nb_2O_5, $Nb_2O_5/iron$, and Nb_2O_5/RGO, have been developed for superior photocatalytic applications. Recently, Nb_2O_5 was coupled with C3N4 to construct heterojunctions for improved H2 production and photocatalytic degradation of organic pollutants. Additionally, Keizo et al. demonstrated the enhanced photocatalytic degradation of the cationic dye, rhodamine B, over $HNb_3O_8/g-C_3N_4$ composite membranes.

Apart from metal oxide semiconductor photocatalysts, polymeric C_3N_4 has recently gained great attraction owing to its remarkable π-conjugates s-triazine structure and narrow band gap of 2.7 eV [21,27]. It utilizes visible light without requiring modifications and exhibits stability in harsh chemical and thermal environments [28]. Moreover, the polymeric nature and planar structure of C3N4 enable its interactions with various substrates [22,29]. C_3N_4 has been successfully coupled with other semiconductors to construct heterojunctions such as C_3N_4–TiO_2 [30,31], C_3N_4–ZnO [32–34], C_3N_4–CdS [35], C_3N_4–$SrTiO_2$ [30,31], C_3N_4–Bi_2WO_6 [36], C_3N_4–$BiVO_4$ [37], $FeCoSe_2/C_3N_4$ [38] etc. Similarly, Nb2O5, a widely studied wide bandgap semiconductor, exhibits high photo-catalytic activity and photostability due to its Brønsted and Lewis sites at the surface, which serve as anchoring points for interacting species [39] [34,40–42]. To extend the absorption spectrum of Nb_2O_5 beyond UV region it is widely coupled with other semiconductor systems such as Nb_2O_5/CuO [43], Nb_2O_5/ZnO [44], TiO_2/Nb_2O_5 [45,46], $Nb_2O_5/iron$ [47] and Nb_2O_5/RGO [48] etc. where heter-ojunction materials exhibited improved catalytic activity in photo redox reactions. Recently Nb_2O_5 was coupled with C_3N_4 to construct heterojunctions for improved H_2 production and photocatalytic degradation of the organic pollutants [49]. Additionally, Keizo et al. demonstrated the enhanced photocatalytic degradation of the cationic dye, rhodamine B, over $HNb_3O_8/g-C_3N_4$ composite membranes [50].

Keeping these studies in view, this work reports the synthesis of C_3N_4/Nb_2O_5 heterojunctions and their efficacy in the photo-catalytic degradation of levofloxacin under visible light. Various mass ratios of C_3N_4 and Nb_2O_5, ranging from 9:1 to 3:7, were investigated to determine the most photoactive heterostructure. Nb_2O_5 facilitates the absorption of levofloxacin, and C_3N_4 extends the absorption regime of the photocatalyst. This synergy led to a significant improvement in the performance of the coupled photocatalyst system. The impact of experimental parameters such as pH, optimal catalyst amount, oxidants and reformation was investigated. Moreover, photodegradation tests under direct sunlight were conducted to reflect the application potential of developed photo-catalysts in real environmental conditions.

2. Experimental

2.1. Synthesis of C_3N_4

C_3N_4 was prepared by the thermal polymerization of melamine ($C_3H_6N_6$) in a muffle furnace at 1 atmospheric pressure. In this procedure, 10g of melamine powder was placed in a crucible covered with another crucible, wrapped with aluminium foil, and heated at 550 °C, for 4 h, at the increasing rate ramp 3 °C, min^{-1}. After that, it cooled gradually at room temperature. The obtained yellow material was then milled and stored for further use.

2.2. Synthesis of Nb_2O_5

Niobium pentoxide Nb_2O_5 nanoparticles were synthesized employing the hydrothermal method. In a typical procedure, in water (35 mL) and triethylamine TEA, (1.0 mL) mixture of 500 mg of $NbCl_5$ was added under constant stirring at 500 rpm at 90 °C and the solution was kept for 1 h until the uniform suspension was obtained. With the dropwise addition of NH_4OH (5 M) pH of the suspension was maintained at 7.5 and then stirred for more than 2 h. The solution was then transferred to a 50 mL Teflon-lined stainless-steel autoclave. The autoclave was placed in an oven at 180 °C for 24 h. The obtained Nb_2O_5 was then collected, dried, and stored for further use.

2.3. Synthesis of C_3N_4/Nb_2O_5 heterojunctions

The heterojunctions of C_3N_4/Nb_2O_5 were prepared using the hydrothermal method, where the procedure for synthesizing Nb_2O_5 was followed, except that C_3N_4 was additionally charged at the outset. A schematics representation of the process is shown in Fig. 1. In

a typical procedure, C_3N_4 was dispersed in water (35 mL) along with TEA (1.0 mL) and subsequently, $NbCl_5$ was dissolved at 90 °C with vigorous stirring until the uniform suspension was obtained. To control the pH of the mixture, NH_4OH (5 M) was added gradually into the suspension until the pH reached 7.5 and then stirred for 2 h. The prepared mixture was transferred to a Teflon-line steel autoclave and placed in the oven for 24 h at 180 °C. After that, the resultant product was washed 3 times with hot deionized water and 2 times with ethanol and collected via centrifugation at 4500 rpm for 5 min. Then the product was dried in an oven at 80 °C. Similarly, different mass ratios of C_3N_4 and Nb_2O_5 were prepared by changing the C_3N_4 amount at the outset and represented as $9C_3N_4/1Nb_2O_5$, $7C_3N_4/3Nb_2O_5$, $6C_3N_4/4Nb_2O_5$, $5C_3N_4/5Nb_2O_5$, and $3C_3N_4/7Nb_2O_5$ respectively. The prepared heterojunctions were ground well and stored for further use.

2.4. Characterization of material

X-ray diffractions (XRD) patterns were measured on a PAN analytical X'Pert Pro diffractometer operating in Bragg–Brentano focusing geometry and using Cu Ka radiation (k = 1.5418 Å) from a generator operating at 40 kV and 40 mA. Transmission electron microscopy (TEM) images and selected area electron diffraction (SEAD) patterns were recorded on JEOL 2010 equipped with a high-resolution pole piece running at 200 kV accelerating voltage. Samples were prepared by dispersing the powder products as a slurry in 1:1 water ethanol solution which was then sonicated for 10 min before being deposited and dried on Agar Scientific 400 mesh Cu holey carbon support. SEM images were taken on JEOL 6500F FEG SEM with a voltage of 5 KV and a working distance of 10 mm. XPS measurements were done using a Thermo Scientific K-Alpha XPS instrument equipped with a micro-focused monochromated Al X-ray source. The source was operated at 12 keV, and a 400 μ spot size was used. Charge neutralization was applied using a combined low energy/ion flood source. The data acquisition was performed with Thermo Scientifics Advantage software, and data analysis was performed with Igor Pro along with XPS fit procedure. UV–vis spectra of the prepared samples were recorded at room temperature with UV–vis NIR spectrophotometer UV-3600 plus. Photoluminescence spectra were obtained with the help of an iHR320 spectrophotometer by Horiba. The PL was collected using a high-resolution monochromator and hybrid photomultiplier detector assembly. The samples were prepared by mixing 0.1g of photocatalyst in dimethylformamide (DMF) containing 50 μL of terpineol and stirring for 5 h. The resulting suspension was coated on a glass substrate at room temperature, followed by drying at 80 °C on a hot plate and annealing at 180 °C for 1 h in a quartz tubular furnace. Spin trapping experiments were performed to detect reactive oxygen species in solution. The measurements were made with a Magnettech MS400 spectrometer and samples were irradiated in in-situ using 300 Xe lamp with 395 cut-off filter. A 10 mg of 5,5-Dimethyl1-pyrroline N-Oxide (DMPO) was added in 1 mL of reaction solution followed by its extraction in a 50 μL aliquot, placed in EPR tube and measured. GCMS spectra were recorded on GC-6890 Agilent Technologies attached with MSD-5973 maintaining mobile phase flux 0.3 ml/min and 5 μL of sample injected volumes.

2.5. Evaluation of photocatalytic tests

Photocatalytic degradation of Levofloxacin was performed using a 300 W Xe arc lamp with a cut-off filter to allow light only $> \lambda = 400$ nm. A stock solution of 30 mg L-1 was prepared using pure levofloxacin powder. Before the experiment, the solution was placed in the dark under continuous stirring for 1 h to achieve adsorption-desorption equilibrium between the pollutant and catalysts. For the photocatalytic experiment, a 50 mL solution of levofloxacin with a concentration of 30 mg/L was taken in a round bottle flask. Solutions were prepared to determine the optimal catalyst dose by adding 0.25 g/L-2.5 g/L of catalysts to water containing 0.1 N HCl. Samples were collected every 30 min, filtered, and analyzed using a UV–Visible absorbance spectrophotometer. The range of catalytic amount, pH, and initial pollutant concentration was tested for optimization of the study. The percentage degradation (%) was calculated using the equation:

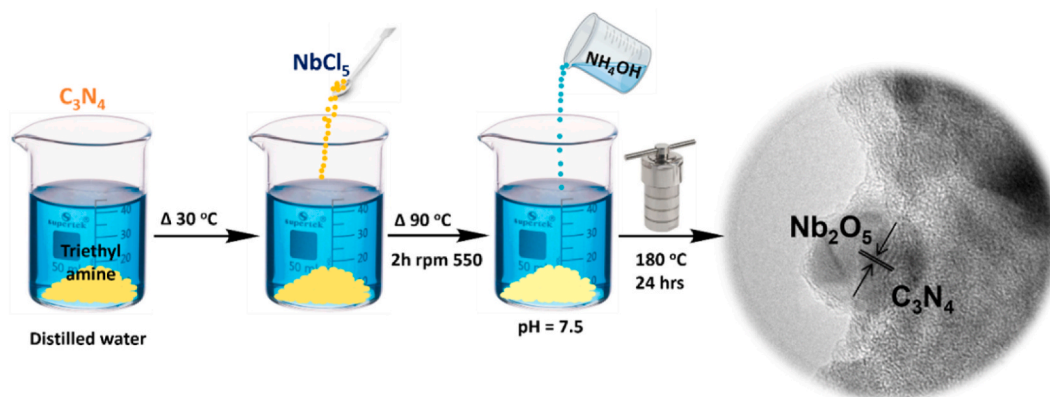$$\text{Efficiency } (\%) = C_0 - C/C_0 \text{ x } 100 \qquad (1)$$

Fig (1). Schematics of hydrothermal synthesis of C_3N_4/Nb_2O_5 heterostructures.

Where C_0 is the initial concentration of the pollutant, and C is the final concentration after photocatalytic degradation.

The experiments were conducted at pH 3 to 10 to determine the best working pH and point of zero charge (PZC). First, 0.1 N solutions of HCl and NaOH were prepared in DI containing catalysts and pH were adjusted to pH 2, 4, 6, 8, 10 and 12. The catalytic solutions with adjusted pH were left for 24 h at room temperature in dark. Afterwards, pH of catalytic solutions was measured with pH meter. PZC was determined by comparing the adjusted pH and pH change.

3. Results and discussion

3.1. Physicochemical properties

The XRD pattern of as-prepared C_3N_4, Nb_2O_5 and C_3N_4/Nb_2O_5 heterojunctions are presented in Fig. 2. The pristine C_3N_4 exhibits two prominent peaks at 13.04° and 27. 4° can be indexed as the (100) and (002) diffractions planes, respectively. These peaks correspond to in-plane structural packing motifs with a d-spacing of d = 0.697 Å, which is slightly smaller than one tri-s-triazine unit (~0.713 Å), and an interlayer stacking distance of d = 0.329 Å of conjugated aromatic systems [51,52]. The prominent diffraction peaks of Nb_2O_5 nanospheres follow the XRD pattern of bulk Nb_2O_5 oxide, although poor crystallinity with broad peaks suggests a small sample size. In addition, the main peaks ascribed to (−111), (111) and (−311) planes are shifted to smaller angles, which indicate a lower number of interconnected Nb–O polyhedra and a less robust structure [41]. After coupling the two semiconductors to form C_3N_4/Nb_2O_5 heterojunction, the characteristic C_3N_4 and Nb_2O_5 peaks are present, suggesting individual crystal structures remained unaltered. Besides the C_3N_4 layer being too thin and the size of Nb_2O_5 being small, the intensities of individual C_3N_4 and Nb_2O_5 diffractions change following the variation in their relative contents in the heterostructure.

The SEM images revealed that Nb_2O_5 exhibited an agglomerated morphology, while C_3N_4 displayed a relatively smooth surface with a lamellar structure lacking clearly defined boundaries (Fig. 3a–b). In contrast, the morphology of the C_3N_4/Nb_2O_5 composite was significantly different from that of C_3N_4 and Nb_2O_5, indicating changes in morphology in heterojunction materials (Fig. 3c). Similarly, high-resolution TEM images (Fig. 3d) of pristine C_3N_4 showed typical aggregated large size morphology and a relatively smooth and flat surface structure. Fig. 3e showed monodispersed Nb_2O_5 nanospheres with a 5–10 nm diameter.

The HRTEM image of $6C_3N_4/4Nb_2O_5$ (Fig. 3f) revealed two distinct phases where the intimate interface between C_3N_4 and Nb_2O_5 and well-matched heterostructure is evident. As seen in XRD, the (100) plane diffraction is less intense, which makes the identification of fringes in C_3N_4 difficult. However, the observed lattice fringe d = 0.304 nm attributed to the (−311) crystallographic plane of the monoclinic Nb_2O_5 system agrees with XRD results. This close interconnection is favourable for necessary charge transfer between coupled semiconductors to promote the separation of photogenerated electron-hole pairs, subsequently improving photocatalytic activity. This close interconnection is favourable for necessary charge transfer between coupled semiconductors, which promotes the separation of photogenerated electron-hole pairs, subsequently enhancing photocatalytic activity.

3.2. Optical properties

The UV–vis absorption spectra of C_3N_4, Nb_2O_5, and C_3N_4/Nb_2O_5 heterostructures are depicted in Fig. 4a. Pure C_3N_4 shows an absorption onset at 470 nm, while Nb_2O_5 absorbs in the ultraviolet (UV) region. An increase in Nb_2O_5 in the C_3N_4/Nb_2O_5 composites resulted in a progressive blue shift. All coupled materials absorb in the visible region and exhibit good absorption intensity. The band gap of the materials was estimated using the equation
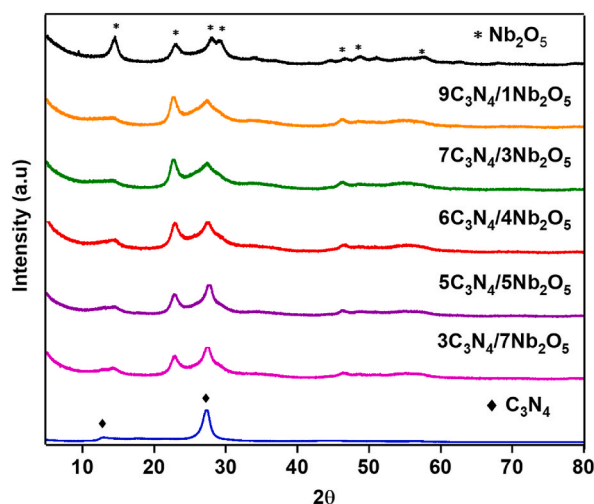

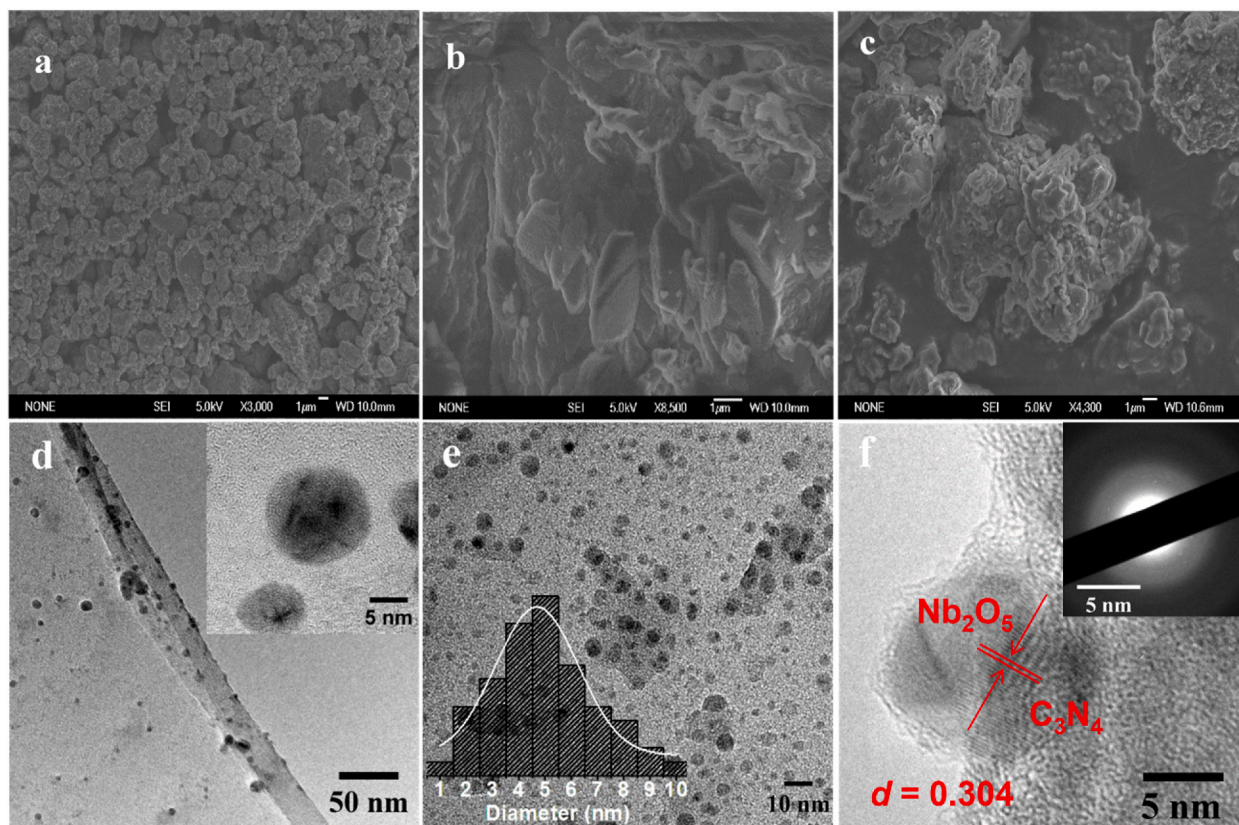**Fig. 2.** XRD patterns of C_3N_4, Nb_2O_5 and heterostructured C_3N_4/Nb_2O_5 materials.

Fig. 3. SEM images of (**a**) Nb_2O_5, (**b**) C_3N_4, (**c**) $6C_3N_4/4Nb_2O_5$ samples. The TEM images of (**d**) C_3N_4, (**e**) Nb_2O_5 particles with a particle size distribution, and (**f**) HR-TEM image of $6C_3N_4/4Nb_2O_5$.

$$\alpha h\upsilon = A(h\upsilon - Eg)^n \tag{2}$$

Where α is the absorption coefficient, $h\upsilon$ is the energy of the photon, Eg is band gap energy, and A is the absorption coefficient (Kubelka-Munka function). The value of n is defined by the characteristics transition of the prepared materials. With the plot of $(\alpha h\upsilon)^{1/2}$ vs $h\upsilon$, obtained band-gap energy of C_3N_4, Nb_2O_5 and heterostructured C_3N_4/Nb_2O_5 is shown in Fig. S1. The estimated values of 2.7 eV for C_3N_4 and 3.54 eV for Nb_2O_5 are consistent with previous reports. After combining the C_3N_4 and Nb_2O_5 semiconductors, the values of the composite are in a range between 2.684 eV and 2.82 eV, confirming that all C_3N_4/Nb_2O_5 composites can absorb the visible part of the solar spectrum. To investigate the charge transfer behavior and charge separation efficiency of charge carriers, we performed
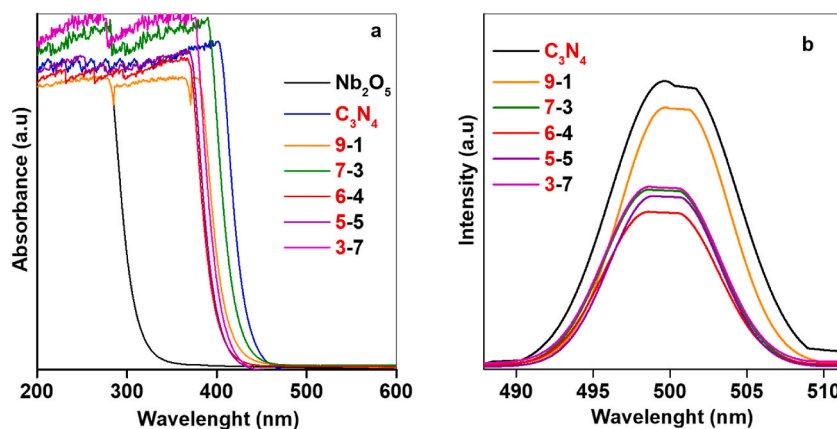

Fig. 4a. UV–Vis spectroscopy of photocatalysts C_3N_4, Nb_2O_5, $9C_3N_4/1Nb_2O_5$, $7C_3N_4/3Nb_2O_5$, $6C_3N_4/4Nb_2O_5$, $5C_3N_4/5Nb_2O_5$ and $3C_3N_4/7Nb_2O_5$. (**b**) Photoluminescence of as-prepared catalysts C_3N_4, Nb_2O_5 and heterostructured C_3N_4/Nb_2O_5 with different mass ratios.

photoluminescence (PL) measurements. Fig. 4b shows the room temperature emission PL spectra of all C_3N_4/Nb_2O_5 heterojunctions measured under the excitation wavelength of 405 nm. A broad emission band between 490 and 510 nm appeared in all C_3N_4/Nb_2O_5 heterojunctions due to the radiative recombination of free electrons in shallow traps and sub-bands underneath the conduction band and free holes at the valence band edge [53,54]. Signal intensities attenuated with the loading ratio between C_3N_4/Nb_2O_5, suggesting the existence of additional energy levels due to heterojunctions that suppress radiative recombination.

3.3. Evaluation of photocatalytic activity

The photocatalytic degradation of levofloxacin over C_3N_4, Nb_2O_5 and C_3N_4/Nb_2O_5 heterojunction composites was evaluated under visible light ($>\lambda = 400$ nm) and results are presented in Fig. 5a–c. The absence of a photocatalyst led to a negligible change ($\sim 8\%$) in levofloxacin concentration in 2 h, indicating minimal photo-degradation. Adsorption tests showed that Nb_2O_5 had a preferential uptake of levofloxacin (21%) compared to C_3N_4 (6%), presumably due to the inherent surface acidity of Nb_2O_5 (Fig. 5d) [34]. However, both C_3N_4 and Nb_2O_5 showed low degradation of 56% and 30% of levofloxacin after 2 h of irradiation. All the heterojunction materials exhibited higher degradation of levofloxacin. The change in absorption spectra for $6C_3N_4/4Nb_2O_5$ showed a gradual decrease in the peak intensity of levofloxacin with longer irradiation time, and no new peaks appeared in the visible or ultraviolet region. Fig. 5b presents the relative levofloxacin concentrations (C/C_0) with irradiation time over heterostructured photocatalysts. After combining C_3N_4 and Nb_2O_5, a significant enhancement in degradation activity for C_3N_4/Nb_2O_5 heterostructures was observed compared to constituent semiconductors, despite Nb_2O_5 not absorbing visible light. The activity increased from $9C_3N_4/1Nb_2O_5$ to $6C_3N_4/4Nb_2O_5$ and decreased drastically afterwards, suggesting the optimal amount of coupled materials. The highest activity was obtained over $6C_3N_4/4Nb_2O_5$, which showed $\sim 72\%$ degradation of levofloxacin in 2 h under visible light irradiation.

This significant improvement in activity was likely due to the synergy of the construction of heterojunction and interface formation, unique Lewis basic sites of carbon nitride surface, and intrinsic Lewis acid sites in Nb_2O_5, thus enhancing surface reactivity [55]. The quantitative assessment of levofloxacin photodecomposition on the photocatalyst surface was calculated using relation

$$-\ln(C / C_0) = kt \qquad (3)$$

where k is rate constant (min^{-1}), C_0 is the initial concentration of dye and c is the actual concentration of target dye at irradiation time t and results are summarized in Table 1 [56]. The apparent rate constant 0.01558 min-1 shown in Fig. 5c was significantly faster for heterojunctions than those of individual C_3N_4 (0.00657 min-1) or Nb_2O_5 (0.00287 min-1). The highest photodegradation rate constant exhibited by $6C_3N_4/4Nb_2O_5$ was twice the rate of C_3N_4 and five times the rate of Nb_2O_5, respectively. This enhancement implies that
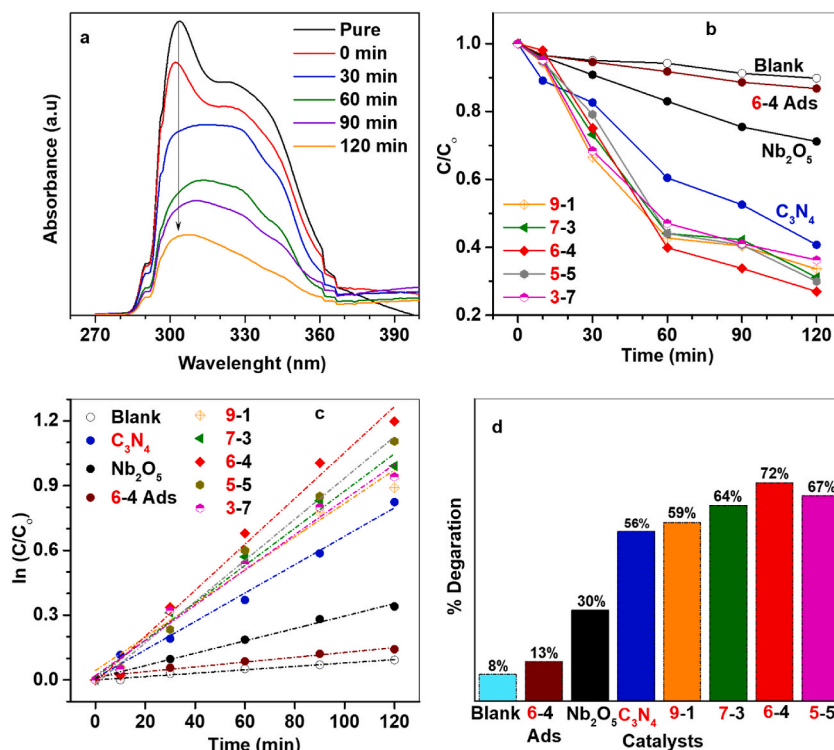

Fig. 5. (a) UV–Vis spectra with a time interval of 30 min (b) C/C_0 Vs Time plots (c) Rate of reactions (d) Percentage degradation of LVX by prepared catalysts.

the coupling of C_3N_4 and Nb_2O_5 results in a synergic electronic structural modification that facilitates the oxidation of levofloxacin, as seen in previous reports [57,58]. The necessity of good interconnection forming heterojunction was confirmed with experiments using a mechanically mixed $6C_3N_4/4Nb_2O_5$ system as a reference, which showed almost similar photocatalytic activity to C_3N_4. This result highlighted the need for an intimate interface in $6C_3N_4/4Nb_2O_5$ heterojunction rather than mechanical mixing for improved activity (Fig. S3†).

3.4. Effect of independent parameter on photocatalytic activity

The catalytic system was optimized by varying parameters such as catalyst amount, levofloxacin concentration, and pH. The results are depicted in Fig. 6a–b. The point of zero charge (PZC) for the C_3N_4/Nb_2O_5 was 6.5, where the catalyst behaves neutrally (Fig. 6b). Above and below the PZC, the catalyst behaves negatively charged and positively charged, respectively. Since the charge of the catalyst is vital concerning the charge of the pollutant (levofloxacin) in water, the photocatalyst showed the best performance at pH = 4 and poor performance at pH = 10, as shown in Fig. 6b. This is owing to the added attraction between opposite charges, in contrast to the negative charge (of photocatalyst and pollutant at high pH) that repel each other [59]. The point of zero charge (PZC) calculated for catalyst is 6.5 suggests that at this pH surface of catalyst behaves neutral. Below this pH surface attains a positive charge and attracts levofloxacin highlighting the reason for high catalytic activity at low pH. Moreover, the optimal concentration of the photocatalyst was obtained by testing the concentration range from 0.25 g/L to 2.5 g/L. The highest activity was observed at 1.5 g/L, which followed a trend of 1.5 (76%) > 2.5 g/L (73%) > 1 g/L (70%) > 0.25 g/L (30%), as shown in Fig. S2. Beyond 1.5 g/L concentration, the decline in activity is due to opacity, which obstructs efficient light penetration. Similarly, the optimum levofloxacin concentration was 12 mg/L with 1.5 g/L and pH = 3, which showed 86% degradation activity. Low efficiency with higher concentrations suggests that the active sites of the photocatalyst saturate above this point. In addition, bubbling O_2 boosted degradation activity to 91%. With bubbling O_2 and adding H_2O_2 together exhibited a slight increase in activity (94%). The excellent activity of the catalytic system (71%) under natural conditions (clear sunny day, solar Lux = 94K, 1 atm. Air, 2h) reflects the practical viability of the system, while photolysis results over an extended period showed no significant change.

It has been noted that structural modifications are typically transient, and reformulation takes place over an extended period. To eliminate this possibility, the reformulation of levofloxacin was examined after two weeks, and no variation was discerned in the trend evident in both samples (Fig. S3). A low degree of absorption associated with the half-life of levofloxacin substantiates the permanence of photocatalytic oxidation, signifying that no reformulation took place.

3.5. Evaluation of photocatalytic and stability

The results reveal the synergetic role of C_3N_4 and Nb_2O_5 in heterojunction configuration. Where preferential adsorption of levofloxacin on the Nb_2O_5 (21% adsorption) surface facilitates the formation of bound species to the surface of the photocatalyst that is crucial for charge injection upon irradiation, while C_3N_4 extends the absorption spectrum of the composite heterojunction. The study also compared the levofloxacin oxidation activity of the C_3N_4/Nb_2O_5 heterojunction with that of a carbon nitride-TiO_2 heterojunction, a wide band gap semiconductor. The results showed that the levofloxacin oxidation activity was lower in the carbon nitride-TiO_2 heterojunction (61%), confirming that preferential binding is unique to the C_3N_4/Nb_2O_5 heterojunction.

To rationalize the superior activity of the C_3N_4/Nb_2O_5 heterojunction, the surface chemical environment of the material was studied using X-ray photoelectron spectroscopy (XPS). The study showed that $6C_3N_4/4Nb_2O_5$ had only Nb, O, N, and C (Fig. 7a). The deconvoluted peak positions of Nb 3d 3/2, 5/2 and O 1s peaks, and C 1s and N 1s peaks of C_3N_4 are consistent with respective surface compositions and binding energies match well with the NIST database values (Fig. 7b–e). The absence of a metallic Nb peak around 202.3 eV indicated that only the metal oxide phase was present. The formation of a type-II heterojunction was confirmed by the Mott-Schottky flat band potentials and band gap values for C_3N_4, and the band edge positions of Nb_2O_5 empirical correlation (Ec ≈ 1.23 – Eg (eV)/2 and Ec ≈ 1.23 + Eg(eV)/2) was used (section S2) [60]. Electronically, the conduction band (CB) and valence band (VB) potentials of C_3N_4 (−1.12 eV and 1.58 eV, respectively) were more negative than those of Nb_2O_5 (−0.39 eV and 2.45 eV, respectively), and this resulted in well-matched type-II heterojunctions (Fig. 7g).

It is noteworthy that the calculated CB standard redox potential of Nb_2O_5 was more negative than the standard redox potential of $O_2/{}^\bullet O_2$ (−0.28 eV) [57,61] and more positive than that of $OH^-/{}^\bullet OH$ (2.27 eV). This confirmed that, upon irradiation, both photo-oxidation and photoreduction reactions were energetically possible in the C_3N_4/Nb_2O_5 system. Photo-induced electron transfer from

Table 1
Kinetics of photocatalytic degradation of levofloxacin under solar light.

Catalysts	Band Gap Eg	Adj. R^2	Degradation rate (K min^{-1})	% Degradation
Nb_2O_5	3.3			
C_3N_4	2.67	0.989	$0.00658 \pm 2.1 \times 10^{-3}$	56
9–1	–	0.942	$0.00775 \pm 8.69 \times 10^{-3}$	58
7–3	–	0.973	$0.00876 \pm 6.32 \times 10^{-3}$	64
6–4	–	0.9657	$0.01558 \pm 1.72 \times 10^{-3}$	87
5–5	–	0.994	$0.00971 \pm 4.42 \times 10^{-3}$	67
3–7	–	0.979	$0.00828 \pm 6.49 \times 10^{-3}$	61
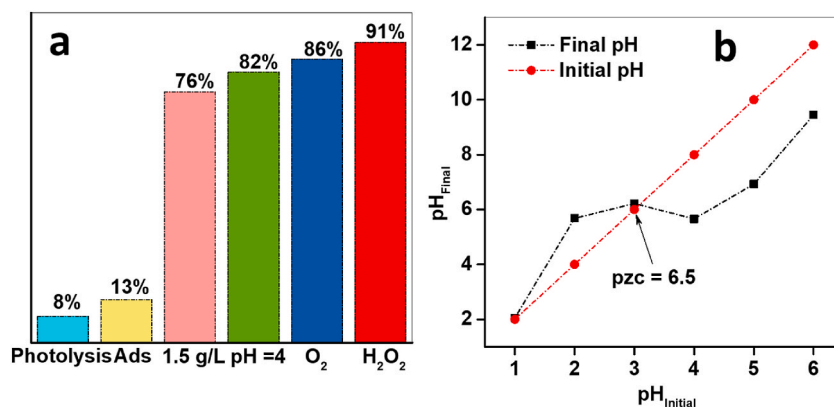
Fig. 6. (a) Effect of optimum pH, catalyst dose, O_2 and H_2O_2 **b)** Point of zero charge (PZC).

the CB of C_3N_4 to the CB of Nb_2O_5 and transfer of holes from the VB of Nb_2O_5 to the VB of C_3N_4 occurred in a concerted manner, which impeded exciton recombination and resulted in improved photoactivity of the heterojunction. The reusability and robustness of the $6C_3N_4/4Nb_2O_5$ heterojunction photocatalyst were examined repeatedly for five cycles. The catalyst exhibited only a slight suppression in activity over time, partly due to quantity of catalyst lost during workup and available oxygen. However, with bubbling oxygen through the reaction mixture restored its reactivity. In addition, examining material structure through XRD before and after the re-action indicated that the photocatalyst structure is chemically stable.

3.6. Mechanism study and fragmentation proposal

Trapping experiments were performed to check the key species involved in levofloxacin degradation. As can be seen in Fig. 8a, adding *tert*-Butyl alcohol (TBA, 2 mM, hydroxyl radical scavenger), degradation rate decreased slightly, suggesting hydroxyl radicals are not key species in the photooxidation of levofloxacin [62]. With the addition of disodium ethylenediaminetetraacetate (EDTA-2Na, 2 mM, holes scavenger), a decrease in rate indicated the involvement of holes in the reaction. Note that photogenerated electrons in CB can reduce O_2 adsorbed to produce superoxide radical ($^\bullet O_2^-$), and holes on VB, by reacting with H_2O, can yield $^\bullet OH$. The addition of benzoquinone (0.5 mM, superoxide radical scavenger) significantly suppressed the degradation rate, indicating that the oxidation of levofloxacin is governed mainly by the $^\bullet O_2^-$ As mentioned above, adding H_2O_2 improved the activity, Raman analysis shows that it alters the Nb_2O_5 surface structure where bands at 640 cm^{-1} are associated with the Nb–O stretching and at 860 cm^{-1} of O–O stretching mode appeared [63,64]. The relative intensity of band (I_{O-O}/I_{Nb-O}) increased with increasing, H_2O_2 and concentration also conform with the observation that $^\bullet O_2^-$ radicals are key species the reaction (Fig. 7f). To confirm the free radicals generated the in solution, spin trapping experiments were performed using 5,5-Dimethyl1-pyrroline N-Oxide (DMPO). Fig. 8b show distinct peaks associated with the generation of $^\bullet O_2^-$ and $^\bullet OH$ radicals at $6C_3N_4/4Nb_2O_5$ photocatalyst surface on irradiation. The high intensity of peaks suggests the efficient production of reactive species.

Based on the observed GC-MS fragmentation data a simplified photocatalytic degradation proposal for levofloxacin is presented in Fig. 8b. GC chromatograms of the main fragments are shown in Fig. S6. As the Levofloxacin may undergo piperazine ring oxidation carbonyl moieties transformation, or decarboxylation, our results are consistent with the previous reports [65,66]. Initial molecular ion peak M+1 ($m/z = 364$) via decarboxylation reaction is transformed into $m/z = 336$ fragment. In addition, an oxidation fragment ($m/z = 304$) associated de-alkylated pathway is also observed. The $m/z = 336$ intermediate via degradation of N-methyl piperazine formed stable intermediate $m/z = 280$ that on hydroxylation, decarboxylation and through the destruction of quinolone moieties in presence of reactive oxygen species leads to the formation of intermediates $m/z = 181$ [66,67]. The compound $m/z = 181$ on defluorination and hydroxylation forms $m/z = 93$ and to subsequent smaller fragments [66,68].

4. Conclusion

In conclusion, the successful construction of heterostructured C_3N_4/Nb_2O_5 photocatalysts has been achieved for the photocatalytic degradation of levofloxacin. Investigations showed that Nb2O5 facilitates the preferential binding of levofloxacin, while C_3N_4 extends the absorption range of the heterostructured catalysts. The type-II heterojunction configuration of the photocatalytic system aided in lowering recombination rates and improved charge transfer. The photocatalytic degradation system C_3N_4/Nb_2O_5 has exhibited remarkable efficiency, removing up to 91% of levofloxacin. Trapping experiments have further revealed that both $^\bullet O_2^-$ radicals and holes drive the degradation of levofloxacin. Additionally, the system has proven to be stable and capable of sustained performance for up to five catalytic cycles.
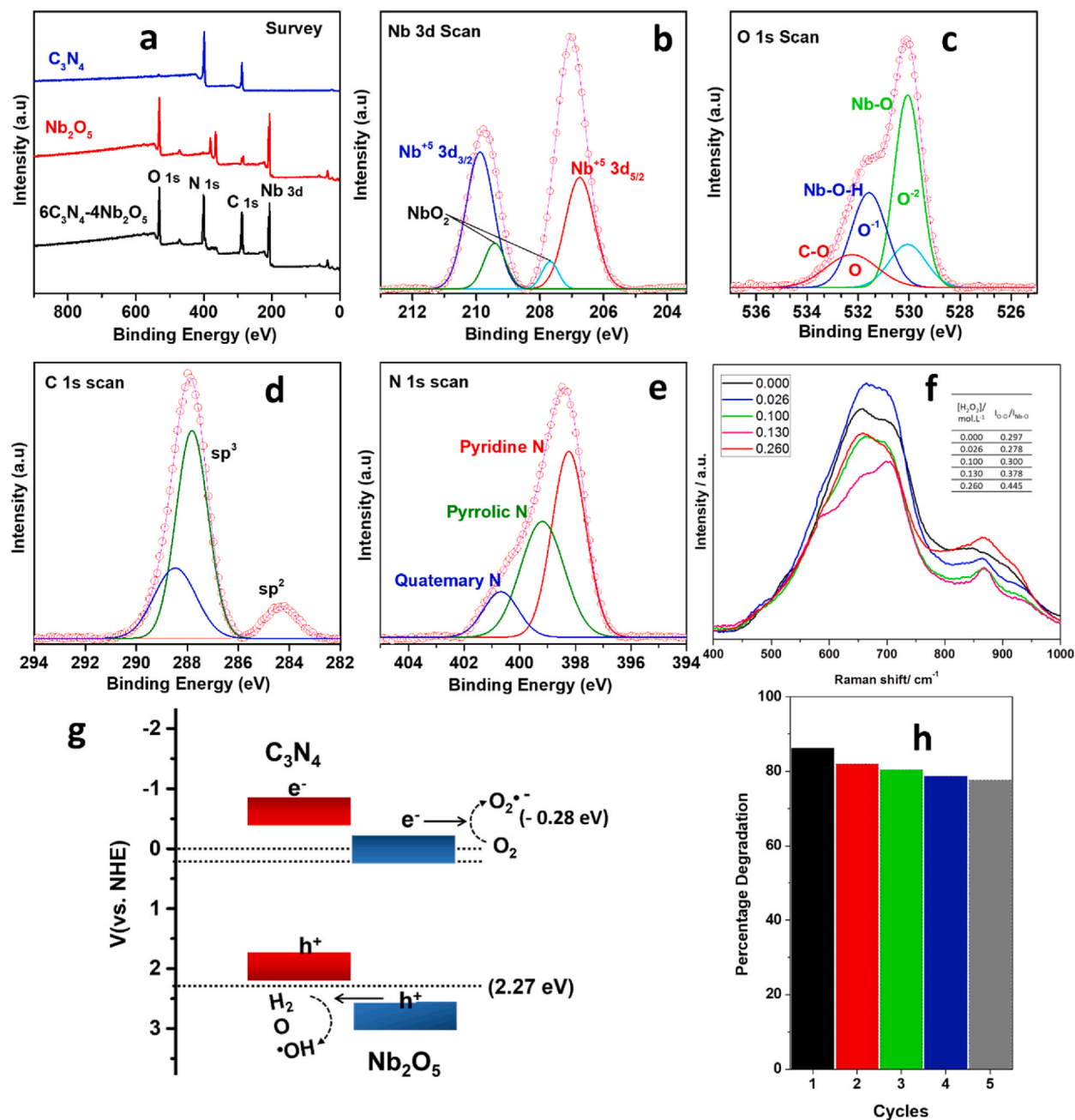
Fig. 7. (**a**) XPS survey spectra of C_3N_4, Nb_2O_5 and $6C_3N_4/4Nb_2O_5$ heterostructure. (**b**) Deconvoluted Nb 3d (**c**) O 1s (**d**) N 1s and (**e**) C 1s scan. (**f**) Change in Raman spectra with H_2O_2 (**g**) Band diagram of $6C_3N_4/4Nb_2O_5$ (**h**) Reusability study of $6C_3N_4/4Nb_2O_5$ photocatalysts.

Authors contributions

Muhammad Imran Rameel and Mehar Wali Performed the experiments; Analyzed, and interpreted the data; analysis; Wrote the paper.

Prof. Dr Jehan Y. Al-Humaidi Contributed reagents, materials, analysis; Wrote the paper.

Faroha Liaqat Analyzed and interpreted the data.

Dr M. Abdullah Khan Conceived and designed the experiments; Analyzed and interpreted the data; Wrote the paper.
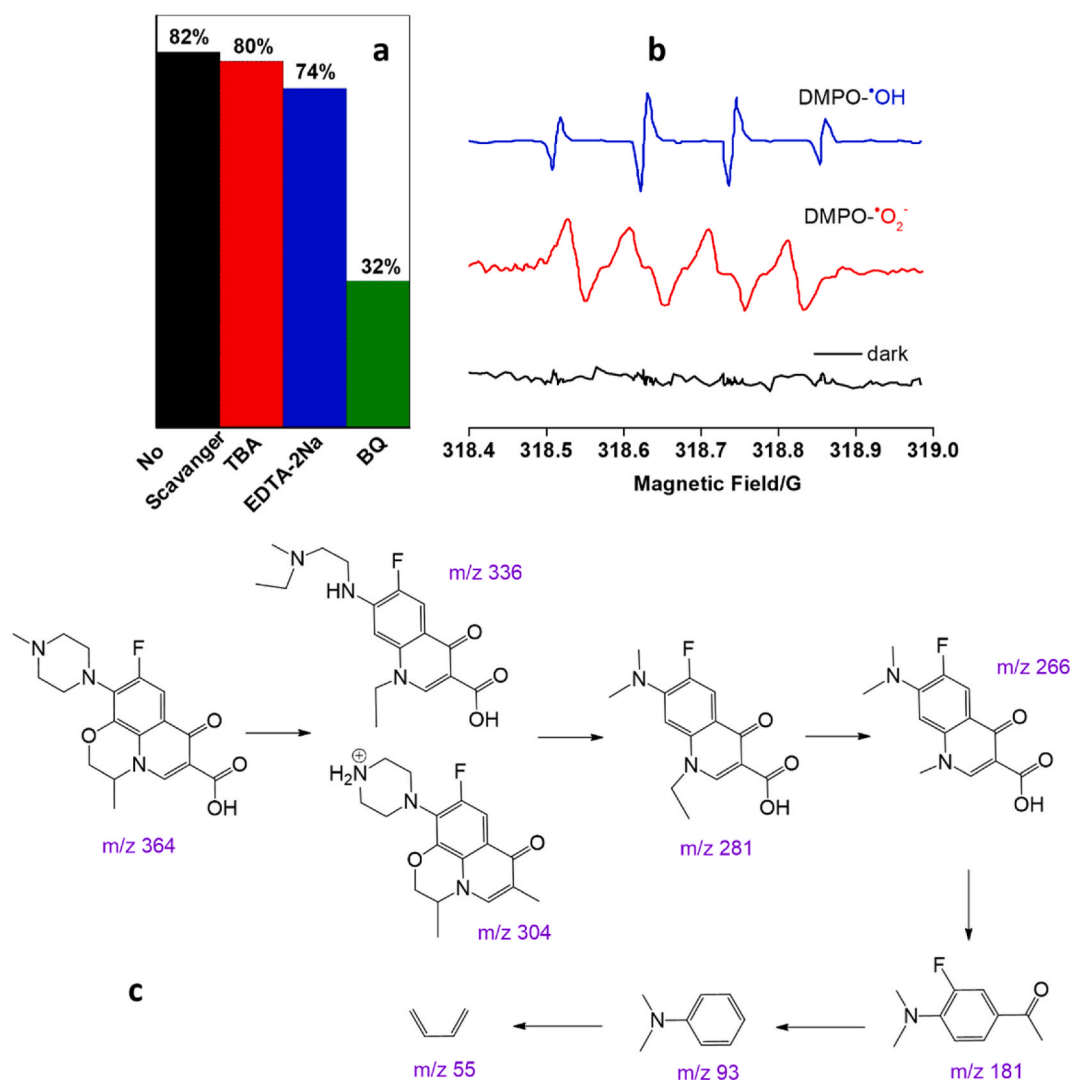
Fig. 8. (**a**) Effect of EDTA-2Na, TBA or BQ addition on the degradation of Levofloxacin over $6C_3N_4/4Nb_2O_5$ heterojunction (**b**) EPR spectra of the (**c**) Proposal for levofloxacin fragmentation pattern during the photocatalytic reaction.

Data availability

Data will be made available on request.

Ethical approval

Not applicable.

Declaration of competing interest

The authors declare that they have no known competing financial interests or personal relationships that could have appeared to influence the work reported in this paper.

Acknowledgements

Appendix A. \Supplementary data

Supplementary data to this article can be found online at https://doi.org/10.1016/j.heliyon.2023.e20479

References

[1] M. Bilal, S. Mehmood, T. Rasheed, H.M.N. Iqbal, Antibiotics traces in the aquatic environment: persistence and adverse environmental impact, Curr Opin Environ Sci Heal 13 (2020) 68–74, https://doi.org/10.1016/j.coesh.2019.11.005.

[2] Z. Maghsodian, A.M. Sanati, T. Mashifana, et al., Occurrence and distribution of antibiotics in the water, Sediment, and Biota of freshwater and marine environments: a review, Antibiotics 11 (2022) 1461, https://doi.org/10.3390/antibiotics11111461.

[3] S. Bhatt, S. Chatterjee, Fluoroquinolone antibiotics: occurrence, mode of action, resistance, environmental detection, and remediation – a comprehensive review, Environ Pollut 315 (2022), 120440, https://doi.org/10.1016/J.ENVPOL.2022.120440.

[4] C.F. Nnadozie, O.N. Odume, Freshwater environments as reservoirs of antibiotic resistant bacteria and their role in the dissemination of antibiotic resistance genes, Environ Pollut 254 (2019), 113067, https://doi.org/10.1016/j.envpol.2019.113067.

[5] O. Alegbeleye, O.B. Daramola, A.T. Adetunji, et al., Efficient removal of antibiotics from water resources is a public health priority: a critical assessment of the efficacy of some remediation strategies for antibiotics in water, Environ. Sci. Pollut. Res. 29 (2022) 56948–57020, https://doi.org/10.1007/s11356-022-21252-4.

[6] M. Mahjoore, M. Honarmand, A. Aryafar, Plant-based green fabrication of CuO-CdO-bentonite S-scheme heterojunction with enhanced photocatalytic performance for the degradation of levofloxacin, Environ. Sci. Pollut. Res. (2023), https://doi.org/10.1007/s11356-023-25277-1.

[7] Q. Yang, Y. Gao, J. Ke, et al., Antibiotics: an overview on the environmental occurrence, toxicity, degradation, and removal methods, Bioengineered 12 (2021) 7376–7416, https://doi.org/10.1080/21655979.2021.1974657.

[8] K.O. Iwuozor, T.A. Abdullahi, L.A. Ogunfowora, et al., Mitigation of levofloxacin from aqueous media by adsorption: a review, Sustain Water Resour Manag 7 (2021) 1–18, https://doi.org/10.1007/s40899-021-00579-9.

[9] M. Handa, W.H. Almalki, R. Shukla, et al., Active pharmaceutical ingredients (APIs) in ionic liquids: an effective approach for API physiochemical parameter optimization, Drug Discov. Today 9 (2022) 2415–2424, https://doi.org/10.1016/j.drudis.2022.06.003.

[10] J. Luo, X. Du, Q. Ye, D. Fu, Review: graphite phase carbon nitride photo-fenton catalyst and its photocatalytic degradation performance for organic wastewater, Catal. Surv. Asia 26 (2022) 294–310, https://doi.org/10.1007/s10563-022-09363-x.

[11] L. Saya, V. Malik, D. Gautam, et al., A comprehensive review on recent advances toward sequestration of levofloxacin antibiotic from wastewater, Sci. Total Environ. 813 (2022), 152529, https://doi.org/10.1016/j.scitotenv.2021.152529.

[12] Z.H. Jabbar, B.H. Graimed, Recent developments in industrial organic degradation via semiconductor heterojunctions and the parameters affecting the photocatalytic process: a review study, J. Water Process Eng. 47 (2022), 102671, https://doi.org/10.1016/j.jwpe.2022.102671.

[13] T. Velempini, E. Prabakaran, K. Pillay, Recent developments in the use of metal oxides for photocatalytic degradation of pharmaceutical pollutants in water—a review, Mater. Today Chem. 19 (2021), 100380, https://doi.org/10.1016/j.mtchem.2020.100380.

[14] S.F. Ahmed, M. Mofijur, B. Ahmed, et al., Nanomaterials as a sustainable choice for treating wastewater, Environ. Res. 214 (2022), 113807, https://doi.org/10.1016/j.envres.2022.113807.

[15] J. Bi, Q. Tao, X. Huang, et al., Simultaneous decontamination of multi-pollutants: a promising approach for water remediation, Chemosphere 284 (2021), 131270, https://doi.org/10.1016/j.chemosphere.2021.131270.

[16] X. Zhang, Y. Gao, Y. Li, et al., Synthesis of magnetic $NiFe_2O_4/CuS$ activator for degradation of lomefloxacin via the activation of peroxymonosulfate under simulated sunlight illumination, Sep. Purif. Technol. 288 (2022) 120664, https://doi.org/10.1016/j.seppur.2022.120664.

[17] S.J. Mazivila, I.A. Ricardo, J.M.M. Leitão, J.C.G.E. da Silva, A review on advanced oxidation processes: from classical to new perspectives coupled to two-and multi-way calibration strategies to monitor degradation of contaminants in environmental samples, Trends Environ Anal Chem 24 (2019), e00072, https://doi.org/10.1016/j.teac.2019.e00072.

[18] R. Nosrati, A. Olad, R. Maramifar, Degradation of ampicillin antibiotic in aqueous solution by ZnO/polyaniline nanocomposite as photocatalyst under sunlight irradiation, Environ. Sci. Pollut. Res. 19 (2012) 2291–2299, https://doi.org/10.1007/s11356-011-0736-5.

[19] M. Ahmaruzzaman, Metal oxides (ZnO, CuO and NiO)-based nanostructured materials for photocatalytic remediation of organic contaminants, Nanotechnol Environ Eng 8 (2022) 219–235, https://doi.org/10.1007/s41204-022-00284-8.

[20] A. Alhebshi, E. Sharaf Aldeen, R.S. Mim, et al., Recent advances in constructing heterojunctions of binary semiconductor photocatalysts for visible light responsive CO_2 reduction to energy efficient fuels: a review, Int. J. Energy Res. 46 (2022) 5523–5584, https://doi.org/10.1002/er.7563.

[21] A. Vázquez, D.B. Hernández-Uresti, S. Obregón, Electrophoretic deposition of CdS coatings and their photocatalytic activities in the degradation of tetracycline antibiotic, Appl. Surf. Sci. 386 (2016) 412–417, https://doi.org/10.1016/j.apsusc.2016.06.034.

[22] L. Lei, W. Wang, Y. Shang, et al., Tailoring chemical structures and intermolecular interactions of melem intermediates for highly efficient photocatalytic hydrogen evolution of g-C_3N_4, Appl. Surf. Sci. 563 (2021), 150384, https://doi.org/10.1016/j.apsusc.2021.150384.

[23] D. Singh, B.R. Gurjar, Recent innovation and impacts of nano-based technologies for wastewater treatment on humans: a review, Environ. Monit. Assess. 195 (2023) 357, https://doi.org/10.1007/s10661-022-10790-6.

[24] M. Asjad, M. Arshad, N.A. Zafar, M.A. Khan, A. Iqbal, A. Saleem, A. Aldawsari, An intriguing case of morphology control and phase transitions in TiO2 nanostructures with enhanced photocatalytic activity, Mater. Chem. Phys. 265 (2021), 124416, https://doi.org/10.1016/j.matchemphys.2021.124416.

[25] N.T.M. Tho, B.T. Huy, D.N.N. Khanh, et al., Visible-light degradation of organic dye based on a heterostructure photocatalyst, Top. Catal. 63 (2020) 1157–1168, https://doi.org/10.1007/s11244-020-01280-5.

[26] N. Rahman, J. Yang, M. Sohail, et al., Insight into metallic oxide semiconductor (SnO_2, ZnO, CuO, α-Fe_2O_3, WO_3)-carbon nitride (g-C_3N_4) heterojunction for gas sensing application, Sensors Actuators A Phys 332 (2021), 113128, https://doi.org/10.1016/j.sna.2021.113128.

[27] Q. Zhang, J. Chen, X. Gao, et al., Enhanced photocatalytic degradation of bisphenol A by a novel donor–acceptor g-C_3N_4: π-π interactions boosting the adsorption and electron transfer behaviors, Sep. Purif. Technol. 300 (2022), 121947, https://doi.org/10.1016/j.seppur.2022.121947.

[28] L.X. Nong, V.H. Nguyen, T. Lee, T.D. Nguyen, Fabrication of g-C_3N_4 with Simultaneous isotype heterojunction and porous structure for enhanced visible-light-driven photocatalytic performance toward tetracycline hydrochloride elimination, Top. Catal. 66 (2022) 275–288, https://doi.org/10.1007/s11244-022-01743-x.

[29] X. Xiao, L. Zhang, H. Meng, et al., Single metal atom decorated carbon nitride for efficient photocatalysis: synthesis, structure, and applications, Sol. RRL 5 (2021), 2000609, https://doi.org/10.1002/solr.202000609.

[30] J. Wang, G. Wang, B. Cheng, et al., Sulfur-doped g-C_3N_4/TiO_2 S-scheme heterojunction photocatalyst for Congo Red photodegradation, Chinese J Catal 42 (2021) 56–68, https://doi.org/10.1016/S1872-2067(20)63634-8.

[31] Z. Wu, Y. Zhao, L. Mi, et al., Preparation of g-C_3N_4/TiO_2 by template method and its photocatalytic performance, Colloids Surfaces A Physicochem Eng Asp 624 (2021), 126756, https://doi.org/10.1016/j.colsurfa.2021.126756.

[32] R. Mohammadzadeh Kakhki, Polymeric organic–inorganic C_3N_4/ZnO high-performance material for visible light photodegradation of organic pollutants, Polym. Bull. (2022), https://doi.org/10.1007/s00289-022-04551-1.

[33] J.-Y. Zhang, J.-Y. Mei, S.-S. Yi, X.-X. Guan, Constructing of Z-scheme 3D g-C_3N_4-ZnO@ graphene aerogel heterojunctions for high-efficient adsorption and photodegradation of organic pollutants, Appl. Surf. Sci. 492 (2019) 808–817, https://doi.org/10.1016/j.apsusc.2019.06.261.

[34] Y. Zhao, C. Eley, J. Hu, et al., Shape-dependent acidity and photocatalytic activity of Nb_2O_5 nanocrystals with an active TT (001) surface, Angew Chemie 124 (2012) 3912–3915, https://doi.org/10.1002/ange.201108580.

[35] M. Pourmadadi, E. Rahmani, M.M. Eshaghi, et al., Graphitic carbon nitride (g-C_3N_4) as a new carrier for drug delivery applications: a review, J. Drug Deliv. Sci. Technol. 104001 (2022), https://doi.org/10.1016/j.jddst.2022.104001.

[36] C. Liu, H. Dai, C. Tan, et al., Photo-Fenton degradation of tetracycline over Z-scheme Fe-g-C_3N_4/Bi_2WO_6 heterojunctions: mechanism insight, degradation pathways and DFT calculation, Appl. Catal. B Environ. 310 (2022), 121326, https://doi.org/10.1016/j.apcatb.2022.121326.

[37] U. Zahoor, M.I. Rameel, A.H. Javed, et al., Yttrium doped bismuth vanadate titania heterojunction for efficient photoreduction of Cr from wastewater under visible light, Int. J. Environ. Res. 16 (2022) 88, https://doi.org/10.1007/s41742-022-00466-x.

[38] X. Xu, J. Zhang, F. Tao, et al., Facile construction of Z-scheme g-C_3N_4/$BiVO_4$ heterojunctions for boosting visible-light photocatalytic activity, Mater. Sci. Eng. B 279 (2022), 115676, https://doi.org/10.1016/j.mseb.2022.115676.

[39] A.G.S. Prado, L.B. Bolzon, C.P. Pedroso, et al., Nb_2O_5 as efficient and recyclable photocatalyst for indigo carmine degradation, Appl. Catal. B Environ. 82 (2008) 219–224, https://doi.org/10.1016/j.apcatb.2008.01.024.

[40] S. Sharma, S. Kumar, S.M. Arumugam, et al., Nb_2O_5/g-C_3N_4 heterojunction facilitates 2, 5-diformylfuran production via photocatalytic oxidation of 5-hydroxymethylfurfural under direct sunlight irradiation, ChemPhotoChem 6 (2022), e202100199, https://doi.org/10.1002/cptc.202100199.

[41] H.T. Kreissl, M.M.J. Li, Y.K. Peng, et al., Structural studies of bulk to nanosize niobium oxides with correlation to their acidity, J. Am. Chem. Soc. 139 (2017) 12670–12680, https://doi.org/10.1021/jacs.7b06856.

[42] Y. Koito, G.J. Rees, J.V. Hanna, et al., Structure–activity correlations for Brønsted acid, Lewis acid, and photocatalyzed reactions of exfoliated crystalline niobium oxides, ChemCatChem 9 (2017) 144–154, https://doi.org/10.1002/cctc.201601131.

[43] A.E. Nogueira, O.F. Lopes, A.B.S. Neto, C. Ribeiro, Enhanced Cr (VI) photoreduction in aqueous solution using Nb_2O_5/CuO heterostructures under UV and visible irradiation, Chem Eng J 312 (2017) 220–227, https://doi.org/10.1016/j.cej.2016.11.135.

[44] Moraes de Np, G.S. dos Santos, G.C. Neves, et al., Development of Nb_2O_5-doped ZnO/Carbon xerogel photocatalyst for the photodegradation of 4-chlorophenol, Optik 219 (2020), 165238, https://doi.org/10.1016/j.ijleo.2020.165238.

[45] X. Bi, G. Du, A. Kalam, et al., Constructing anatase TiO_2/Amorphous Nb_2O_5 heterostructures to enhance photocatalytic degradation of acetaminophen and nitrogen oxide, J. Colloid Interface Sci. 601 (2021) 346–354, https://doi.org/10.1016/j.jcis.2021.05.120.

[46] C.L. Ücker, F.C. Riemke, N.F. de Andrade Neto, et al., Influence of Nb_2O_5 crystal structure on photocatalytic efficiency, Chem. Phys. Lett. 764 (2021), 138271, https://doi.org/10.1016/j.cplett.2020.138271.

[47] C.L. Ücker, V. Goetzke, F.C. Riemke, et al., The photocatalytic performance of Fe inserted in Nb_2O_5 obtained by microwave-assisted hydrothermal synthesis: factorial design of experiments, J. Photochem. Photobiol. Chem. 435 (2023), 114294, https://doi.org/10.1016/j.jphotochem.2022.114294.

[48] B.M.F. Jones, G. Mamba, D. Maruthamani, V. Muthuraj, Honeycomb Nb_2O_5/RGO wrapped on MoO_3 nanorods for visible light-driven degradation of sulfasalazine and ciprofloxacin in water, Colloids Surfaces A Physicochem Eng Asp 653 (2022), 129836, https://doi.org/10.1016/j.colsurfa.2022.129836.

[49] I. Khan, N. Baig, A. Qurashi, Graphitic carbon nitride impregnated niobium oxide (g-C_3N_4/Nb_2O_5) type (II) heterojunctions and its synergetic solar-driven hydrogen generation, ACS Appl. Energy Mater. 2 (2019) 607–615, https://doi.org/10.1021/acsaem.8b01633.

[50] S. Imoto, K. Nakagawa, C. Hu, et al., HNb_3O_8/g-C_3N_4 nanosheet composite membranes with two-dimensional heterostructured nanochannels achieve enhanced water permeance and photocatalytic activity, Chem Eng J 442 (2022), 136254, https://doi.org/10.1016/j.cej.2022.136254.

[51] J. Zhang, M. Zhang, R.-Q. Sun, X. Wang, A facile band alignment of polymeric carbon nitride semiconductors to construct isotype heterojunctions, Angew. Chem. Int. Ed. 51 (2012) 10145–10149, https://doi.org/10.1002/anie.201205333.

[52] Y. Wang, X. Wang, M. Antonietti, Polymeric graphitic carbon nitride as a heterogeneous organocatalyst: from photochemistry to multipurpose catalysis to sustainable chemistry, Angew Chem. Int. Ed. Engl. 51 (2012) 68–89, https://doi.org/10.1002/anie.201101182.

[53] L. Zhang, L. Tan, Z. Yuan, et al., Engineering of $Bi_2O_2CO_3$/Ti_3C_2Tx heterojunctions co-embedded with surface and interface oxygen vacancies for boosted photocatalytic degradation of levofloxacin, Chem Eng J 452 (2023), 139327, https://doi.org/10.1016/j.cej.2022.139327.

[54] W.-J. Ong, L.-L. Tan, Y.H. Ng, et al., Graphitic carbon nitride (g-C_3N_4)-based photocatalysts for artificial photosynthesis and environmental remediation: are we a step closer to achieving sustainability? Chem Rev 116 (2016) 7159–7329, https://doi.org/10.1021/acs.chemrev.6b00075.

[55] Z. Lin, X. Wang, Nanostructure engineering and doping of conjugated carbon nitride semiconductors for hydrogen photosynthesis, Angew. Chem. Int. Ed. 52 (2013) 1735–1738, https://doi.org/10.1002/anie.201209017.

[56] P. Singh, B. Mohan, V. Madaan, et al., Nanomaterials photocatalytic activities for waste water treatment: a review, Environ. Sci. Pollut. Res. 29 (2022) 69294–69326, https://doi.org/10.1007/s11356-022-22550-7.

[57] Y. Tian, B. Chang, Z. Yang, et al., Graphitic carbon nitride–$BiVO_4$ heterojunctions: simple hydrothermal synthesis and high photocatalytic performances, RSC Adv. 4 (2014) 4187–4193, https://doi.org/10.1039/c3ra46079g.

[58] Y. Tian, B. Chang, J. Lu, et al., Hydrothermal synthesis of graphitic carbon nitride-Bi_2WO_6 heterojunctions with enhanced visible light photocatalytic activities, ACS Appl. Mater. Interfaces 5 (2013) 7079–7085, https://doi.org/10.1021/am4013819.

[59] H. Zhang, W. Wu, Y. Li, et al., Enhanced photocatalytic degradation of ciprofloxacin using novel C-dot@Nitrogen deficient g-C_3N_4 : Synergistic effect of nitrogen defects and C-dots, Appl. Surf. Sci. 465 (2019) 450–458, https://doi.org/10.1016/j.apsusc.2018.09.183.

[60] Y. Matsumoto, Energy positions of oxide semiconductors and photocatalysis with iron complex oxides, J. Solid State Chem. 126 (1996) 227–234, https://doi.org/10.1006/jssc.1996.0333.

[61] L. Wu, J.C. Yu, X. Fu, Characterization and photocatalytic mechanism of nanosized CdS coupled TiO_2 nanocrystals under visible light irradiation, J. Mol. Catal. Chem. 244 (2006) 25–32, https://doi.org/10.1016/j.molcata.2005.08.047.

[62] G.V. Buxton, C.L. Greenstock, W.P. Helman, A.B. Ross, Critical review of rate constants for reactions of hydrated electrons, hydrogen atoms and hydroxyl radicals (OH/O−) in aqueous solution, J. Phys. Chem. Ref. Data 17 (1988) 513–886, https://doi.org/10.1063/1.555805.

[63] R.F. Brandão, R.L. Quirino, V.M. Mello, et al., Synthesis, characterization and use of Nb_2O_5 based catalysts in producing biofuels by transesterification, esterification and pyrolysis, J. Braz. Chem. Soc. 20 (2009) 954–966, https://doi.org/10.1590/S0103-50532009000500022.

[64] F. Dubnikova, R. Kosloff, J. Almog, et al., Decomposition of triacetone triperoxide is an entropic explosion, J. Am. Chem. Soc. 127 (2005) 1146–1159, https://doi.org/10.1021/ja0464903.

[65] L. Li, C.G. Niu, H. Guo, J. Wang, M. Ruan, L. Zhang, C. Liang, H.Y. Liu, Y.Y. Yang, Efficient degradation of Levofloxacin with magnetically separable $ZnFe_2O_4$/NCDs/Ag_2CO_3 Z-scheme heterojunction photocatalyst: vis-NIR light response ability and mechanism insight, Chem. Eng. J. 383 (2020), https://doi.org/10.1016/j.cej.2019.123192.

[66] S.L. Prabavathi, K. Saravanakumar, C.M. Park, V. Muthuraj, Photocatalytic degradation of levofloxacin by a novel Sm_6WO_{12}/g-C_3N_4 heterojunction: performance, mechanism and degradation pathways, Sep. Purif. Technol. 257 (2021), 117985, https://doi.org/10.1016/j.seppur.2020.117985.

[67] M.S. Yahya, M. El Karbane, N. Oturan, K. El Kacemi, M.A. Oturan, Mineralization of the antibiotic levofloxacin in aqueous medium by electro-Fenton process: kinetics and intermediate products analysis, Environ. Technol. 37 (2016) 1276–1287, https://doi.org/10.1080/09593330.2015.1111427.

[68] Y. Gong, J. Li, Y. Zhang, M. Zhang, X. Tian, A. Wang, Partial degradation of levofloxacin for biodegradability improvement by electro-Fenton process using an activated carbon fiber felt cathode, J. Hazard Mater. 304 (2016) 320–328, https://doi.org/10.1016/j.jhazmat.2015.10.064.